ISSN 0208-7774 TRIBOLOGIA 6/2020 p. 77–85
DOI: 10.5604/01.3001.0014.8340

Mirosław WITASZEK*, Kazimierz WITASZEK**

WEAR OF RAILWAY TYRE STEELS MODELLING USING ARTIFICIAL NEURAL NETWORKS

MODELOWANIE ZUŻYCIA STALI NA OBRĘCZE KÓŁ KOLEJOWYCH ZA POMOCĄ SZTUCZNYCH SIECI NEURONOWYCH

Key words: wear, tyre steels, artificial neural networks, modelling.

Abstract: In the paper the results of sliding wear tests were used to model the dependence of steel volume loss on railway wheel tyres on selected material parameters and sliding conditions. The material properties included in this modelling were the hardness and chemical composition of the tyre material (specimens) and the hardness of the mating material (counter-specimens). The conditions for sliding were the initial maximum Hertzian pressure and the sliding distance. The tests were carried out in the ring-block system. Artificial neural networks were used for modelling. It was found that the constructed model made it possible to quantify the volume loss from the above–mentioned factors. A clear influence of the pressure, friction distance, and hardness of both cooperating materials on the studied wear was found. The influence of the chemical composition is less noticeable due to the rather narrow range of its allowable changes. The microscopic tests allowed us to identify the main wear mechanisms in the sliding friction of the tested tyre and rail steels.

Słowa kluczowe: zużycie, stale na obręcze kół kolejowych, sztuczne sieci neuronowe, modelowanie.

Streszczenie W pracy przedstawiono wykorzystanie wyników badań zużycia przy tarciu ślizgowym do modelowania zależności zużycia objętościowego stali na obręcze kół kolejowych od wybranych parametrów materiału i warunków współpracy. Własnościami materiału uwzględnionymi w tym modelowaniu były twardość oraz skład chemiczny materiału obręczy (próbki) oraz twardość materiału współpracującego (przeciwpróbki). Warunkami współpracy były początkowy, maksymalny nacisk Hertza i droga tarcia. Badania przeprowadzono w układzie klocek–krążek. Do modelowania wykorzystano sztuczne sieci neuronowe. Stwierdzono, że zbudowany model pozwolił na określenie zależności ilościowych ubytku objętościowego od wyżej wymienionych czynników. Wskazano występowanie wyraźnego wpływ nacisku, drogi tarcia, twardości obu współpracujących materiałów na badane zużycie. Wpływ składu chemicznego jest mniej zauważalny z powodu dość wąskiego zakresu dopuszczalnych jego zmian. Badania mikroskopowe pozwoliły na zidentyfikowanie głównych mechanizmów zużywania przy tarciu ślizgowym badanych stali obręczowych i szynowej.

INTRODUCTION

Wheels and rails are among the elements generating the highest maintenance costs on railroads **[L. 1–4]**. In recent decades, there has been a tendency to increase train speed and axle load, which improves rail transport. However, this makes the conditions for wheel and rail cooperation become more and more severe. This shortens their service life and increases their maintenance costs **[L. 1**, **5–7]**. Therefore, research on the deterioration processes of railway wheels and rails aimed at increasing their lifetime is crucial for railway operators.

The durability of wheels and rails is limited by various deterioration processes. They depend on the conditions of wheel/rail interaction. On a straight track, the interaction of a wheel tread with a rail head is a rolling with some portion of slip. It causes wear, corrugation and the dominant contact fatigue in these conditions: spalling, shelling, and head checks **[L. 2**, **8]**. In a curve, the portion of sliding increases **[L. 2**, **6, 9]**

* ORCID: 0000-0001-7901-2319. Silesian University of Technology, Department of Road Transport, Faculty of Transport, Krasińskiego Street 8, 40-019 Katowice, Poland.
* ORCID: 0000-0002-3105-0532. Silesian University of Technology, Department of Road Transport, Faculty of Transport, Krasińskiego Street 8, 40-019 Katowice, Poland.

when the flange is in contact with the side of the rail head. In the papers **[L. 6**, **8]** it is reported that even pure sliding occurs in such conditions. This leads to an intensification of wear. The tighter the curve, the more intense is the wear **[L. 2**, **6]**. This wear is reduced thanks to material improvement and the use of lubrication of the rails and flanges of the wheels. Nevertheless, wear on the wheel flanges and gauge side of the rail heads can still be a serious problem, especially on heavy haul railroads, in sharp curves and in case of failure of the lubrication **[L. 3, 4, 8]**. As stated in **[L. 10]**, excessive wheel wear also occurs on high-speed railways.

In order for the activities aimed at increasing the durability of wheels and rails to be effective, it is necessary to study wear and contact fatigue processes. These studies include field research **[L. 11, 12]** and laboratory tests. The former are characterized by high costs and other difficulties, so researchers are willing to carry out the latter whenever possible **[L. 4]**. In laboratory tests, devices are sometimes used in which the specimens are of considerable size and reproduce the profiles of wheels and rails **[L. 3, 4, 13]**. Most often, however, they are performed on small-scale test rigs. Typical devices used in such studies are called "twin-disk testers" **[L. 4, 5, 10, 14-22]**. They allow for rolling-sliding friction and wear tests. Such conditions are typical for contact between the wheel tread and the rail head **[L. 2]**. Simulating wheel flange / gauge corner of the rail head interaction is possible on such devices by increasing the creepage **[L. 17]**. Pure sliding testers are also used to test friction and wear in this contact. Among them, the most common are pin-on-disk testers **[L. 2, 8, 23, 24]**. Some researchers use pins with a flat face **[L. 8, 24]**, while others use rounded tip pins **[L. 2, 23]**. The latter make it possible to obtain an initial point contact. In addition to the pin-on-disk testers, there ring-block testers are also used **[L. 6, 7, 25]**. There is a contact between the flat surface of the block and the cylindrical surface of the disc, which is the initial linear contact. Both point and line contacts enable high contact pressure with values equivalent to those in existence.

Rail steels wear was also tested on ball-on-disk testers **[L. 11, 12, 26]**. A comparison of the results of these tests and field researches confirmed that this method allows one to predict wear behaviour, rail crack tendency and the work hardening behaviour. However, it cannot be assessed the life of rails using this method **[L. 12, 14]**.

The results of laboratory tests can be used to model the wear of wheels and rails. For this, the Archard model is often used, which assumes that the volume of worn material is proportional to the wear factor, normal force and friction distance and is inversely proportional to the hardness of the material **[L. 4, 15]**. Such models allow for accurate forecasting of wear **[L. 15]**. Other models use an energy approach where wear is a function of the energy dissipated in contact **[L. 15, 27]**. Their wear is strongly dependent on the sliding speed. They are suitable for predicting rolling contact fatigue, but their usefulness for predicting wear is small **[L. 15]**. The main difficulty in applying the Archard model is the strong dependence of the wear coefficient on contact conditions, which in the case of wheels and rail rails show considerable variability **[L. 15]**. The wear factor of the Archard model also depends on the heat treatment of the material. For example, for heat-treated rails it is smaller than for rails without such treatment **[L. 4]**. The data presented in Ref. **[L. 4]** indicates that it does not depend significantly on the product of stress and slip.

In this study, a wear model was built based on the results of laboratory tests with sliding friction in the ring-block system. It allows one to determine the influence of various factors on wear of tyre steels. Since the hardness of the material of the mating element (rail) was not taken into account in the Archard model, it was decided to use a different model that takes this factor into account. As in Ref. **[L. 3]**, artificial neural networks (ANNs) were used for its construction. Due to the fact that in work **[L. 3]** a different test apparatus was used than in this work (with specimens of large sizes with the wheel and rail profile), a different set of input and output values was adopted for modelling. The input variables were the maximum Hertzian pressure, the sliding distance, wheel and rail hardness, and the chemical composition of the steel on the tyres expressed by the carbon equivalent calculated according to the following formula, given in **[L. 28]**:

$$C_E = C + \frac{4 \cdot Mn}{19} + \frac{Si}{10} \tag{1}$$

where: C, Mn, Si – contents of carbon, manganese and silicon, respectively in wt.%

EXPERIMENTAL DETAILS

Sliding wear tests were carried out on a modified Timken wear testing machine (**Fig. 1a**) in the ring-block system (**Fig. 1b**). As specimens, blocks with dimensions of 10 x 10 x 20 mm made of tyre steels were used. The chemical composition and hardness of the tested steels are presented in **Table 1**.

Two series of experiments were conducted. In the first, the counter-specimen, in the form of a ring, was made of 900A rail steel with a hardness of 34 HRC. In the second, as in the papers **[L. 18–22]**, the counter-specimen was made of 100Cr6 steel with a hardness of 61 HRC. The outer diameter of the counter-specimen in both series was 47 mm.

Data from **[L. 4, 23]** were used to select the test conditions. The contact stress was selected on the basis of the work **[L. 4]** in which it is stated that the maximum Hertzian pressure between the wheel flange and the side

Table 1. Chemical composition and hardness of the tested steels
Tabela 1. Skład chemiczny i twardość badanych stali

No	Steel grade	Chemical composition, wt. %					Hardness
		C	Mn	Si	P	S	HB
1	P54	0.56	0.69	0.22	0.018	0.035	203
2	P54	0.53	0.73	0.22	0.016	0.004	292
3	P55A	0.56	0.70	0.28	0.010	0.005	247
4	P60	0.61	0.79	0.30	0.016	0.004	280
5	P60	0.61	0.76	0.29	0.017	0.006	203

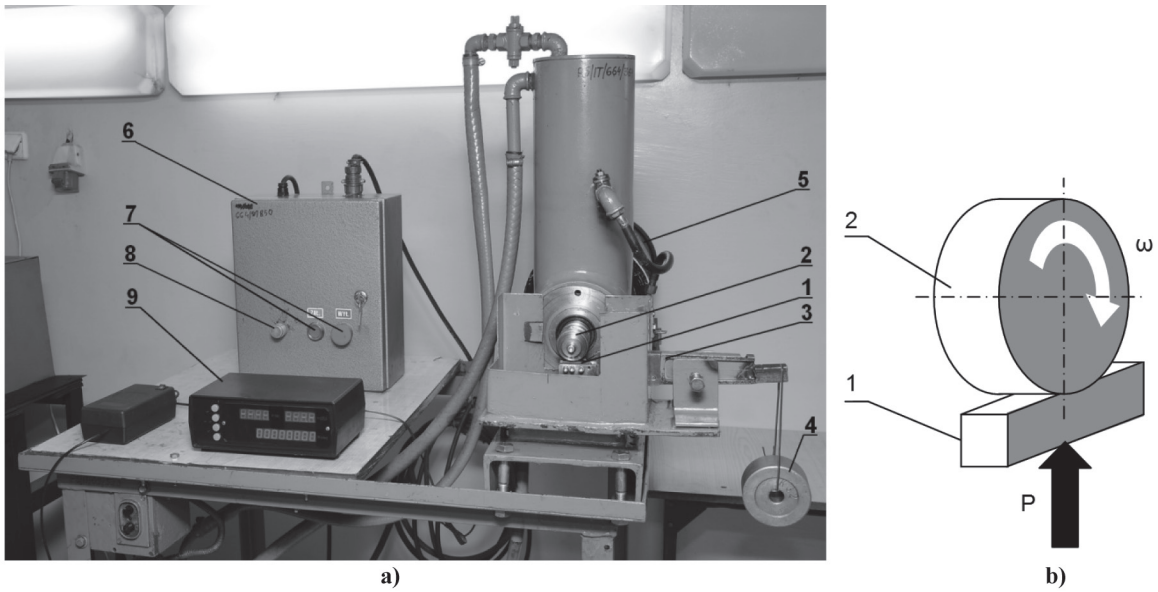

Fig. 1. Modified Timken wear testing machine: a) the appearance: 1 – specimen, 2 – counter–specimen, 3 – first–order lever, 4 – weight, 5 – DC–motor, 6 – motor controller, 7 – switch, 8 – potentiometer for rotating – speed controlling, 9 – counter of revolutions; b) the scheme of the ring-block system: 1 – specimen; 2 – counter-specimen, P – load, ω – angular speed of the counter–specimen

Rys. 1. Zmodyfikowane stanowisko Timkena: a) widok: 1 – próbka, 2 – przeciwpróbka, 3 – dźwignia dwustronna, 4 – obciążnik, 5 – silnik elektryczny prądu stałego, 6 – sterownik silnika, 7 – wyłącznik, 8 – potencjometr regulacji prędkości obrotowej, 9 – licznik obrotów; b) schemat układu klocek–krążek: 1 – próbka, 2 – przeciwpróbka, P – obciążenie, ω – prędkość kątowa przeciwpróbki

of the rail head in the track curve is on average 400 MPa. For rails that are not worn or exhibit significant wear due to rubbing against the flange, these pressures assume lower values. Therefore, the tests were carried out for maximum Hertzian pressures ranging from 98.5 MPa to 434 MPa.

It is stated in the work **[L. 23]** that in the wear tests simulating the contact of the tyre with the side of the rail head, with sliding wear and high initial pressure, as is the case in the ring-block system, particular attention should be paid to the initial section of the sliding distance. Excessive heating of the specimen can then induce changes in wear mechanisms. There is also a reduction in pressure due to the enlargement of the contact area due to wear. Therefore, in this study, a sliding distance ranging from about 0.04 m to 0.74 m was adopted. That corresponds to 0.25–5 revolutions of counter-specimen. Additionally, the heating of the specimen was minimized by performing tests for a low sliding speed of 0.02 m · s^{-1}, which, like in the papers **[L. 8, 11, 12, 24, 26]**, was constant during the research. Due to such low value of sliding speed the repetition of sliding distance was of 5 mm in each test.

RESULTS AND DISCUSSION

Wear of specimens

Examples of wear test results are shown in **Fig. 2**. As can be seen in this figure results are considerably scattered. This results from short sliding distances that were adopted in the present study.

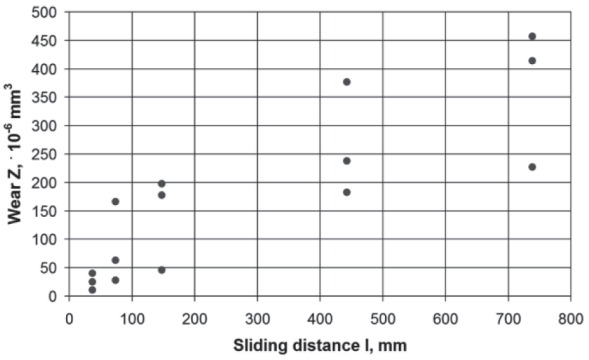

Fig. 2. Wear of specimens made of P60 steel (No. 2 in Table 1) mated with counter-specimen made of 900A steel

Rys. 2. Zużycie próbek ze stali P60 (nr 2 w tabeli 1), w skojarzeniu z przeciwpróbką ze stali 900A

Microscopic observations

Figures 3 and **4** show SEM micrographs of P54 and P60 steel microstructures with hardness of 203 HBW and 280 HBW, respectively. These figures show that the tested steels have a pearlitic-ferritic microstructure.

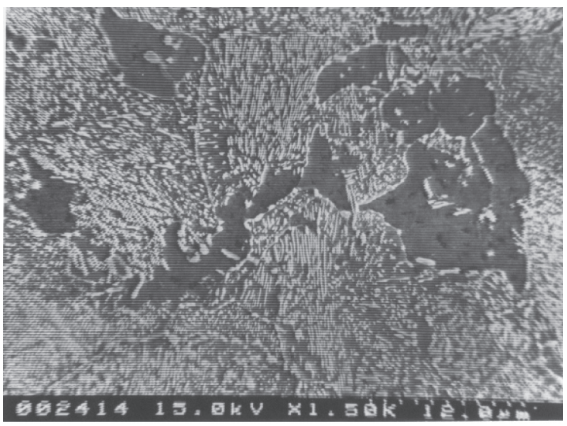

Fig. 3. Microstructure of P54 steel (No. 1 in Table 1). Nital 2%

Rys. 3. Mikrostruktura stali P54 (nr 1 w tabeli 1). Nital 2%

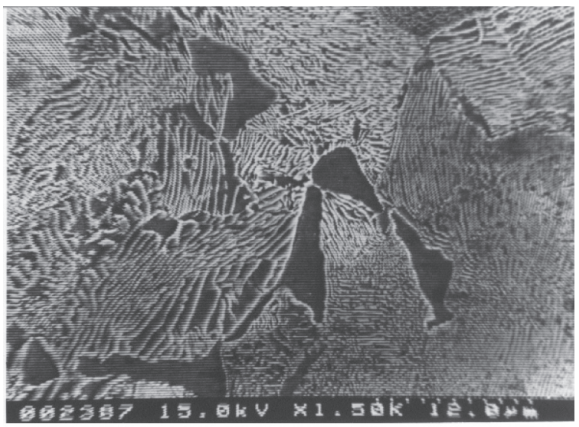

Fig. 4. Microstructure of P60 steel (No. 4 in Table 1). Nital 2%

Rys. 4. Mikrostruktura stali P60 (nr 4 w tabeli 1). Nital 2%

Microscopic examination of worn surfaces was performed to determine the wear mechanisms. **Figure 5** shows a SEM micrograph of the surface of the wear scar of a specimen made of P54 steel with a hardness of 203 HBW after rubbing with a rail steel with a hardness of 34 HRC at a low sliding distance (37 mm). It shows horizontal abrasion scratches in the sliding direction. Similar scratches were observed in the works **[L. 2**, **8]**. They can be caused both by the movement of the asperities of the harder counter-specimen over the specimen surface and by wear products located between the mating surfaces. **Figure 6** shows the worn surface of the specimen, also made of P54 steel, after rubbing with the steel rail with a hardness of 34 HRC at the highest

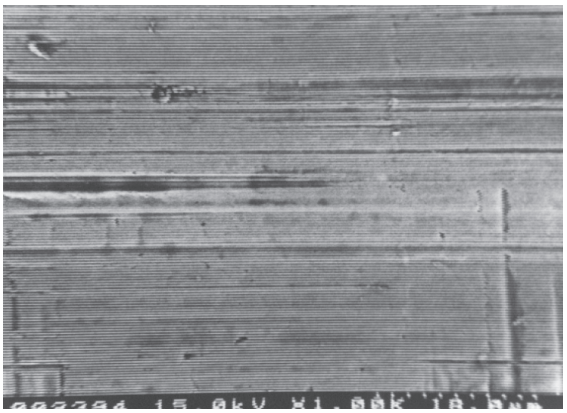

Fig. 5. SEM micrograph of specimens made of P54 steel with a hardness of 203 HBW after rubbing against rail steel of a hardness of 34 HRC at a sliding distance of 37 mm

Rys. 5. Mikrofotografia skaningowa próbki ze stali P54 o twardości 203 HBW po współpracy ze stalą szynową o twardości 34 HRC przy drodze tarcia 37 mm

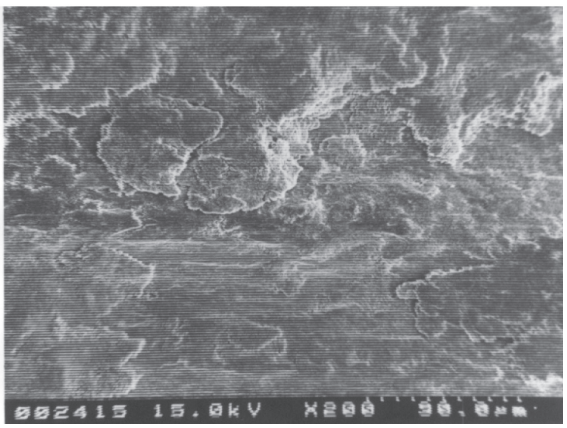

Fig. 6. SEM micrograph of the worn surface of specimen made of P54 steel with a hardness of 203 HBW after rubbing against rail steel of a hardness of 34 HRC at the sliding distance of 738 mm

Rys. 6. Mikrofotografia skaningowa zużytej powierzchni próbki ze stali P54 o twardości 203 HBW po współpracy ze stalą szynową o twardości 34 HRC przy drodze tarcia 738 mm

tested sliding distance (738 mm). According to papers **[L. 6, 7]**, the appearance of the specimen surface is typical for material spalling. It is caused by plastic deformation that promotes crack initiation and propagation in the surface layer of material **[L. 16]**. This is facilitated by the presence of ferrite, which, after deformation, forms layers approximately parallel to the surface. The fatigue crack grows along with this ferrite layer and then the material above the crack fractures forming flake-like wear particle **[L. 16]**. These products oxidize fairly quickly **[L. 2]**. Oxidized particles, can adhere to the disc surface and cause abrasive wear **[L. 2]**.

Wear modelling

To properly carry out the process of training neural networks, it is necessary to prepare two data sets containing many examples of sets of input parameters and the corresponding wear. They were prepared on the basis of the results of the conducted wear tests. The model takes into account the five input parameters mentioned above (Hertz pressure, sliding distance, specimen hardness, counter-specimen hardness and carbon equivalent) and one output variable – specimen wear. The research results included 594 data records, 518 of which were used to train the network. A test set was created from the remaining 76 records. The process of creating, learning and testing the network was carried out with the use of free SNNS software, which was enriched with the user's own software (**Fig. 7**). Thanks to this integration, much more control over the learning process was gained. Another important modification was the automatic creation of charts using scripts and the Gnuplot program.

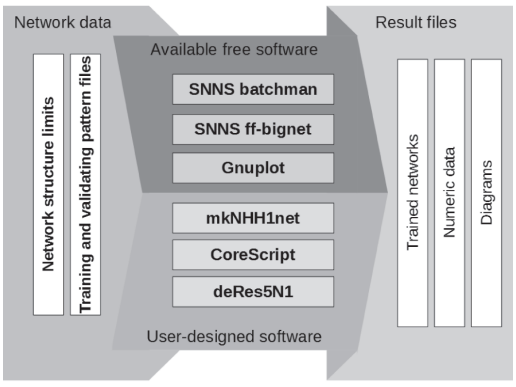

Fig. 7. Data processing scheme
Rys. 7. Schemat obróbki danych

On the basis of preliminary experiments, it was decided to use a feed-forward network with a structure containing two hidden layers in addition to the input and output layers. Such networks are capable of generalizing knowledge significantly. Due to the number of selected parameters, 5 neurons were used in the input layer and one neuron worked at the output. The first hidden layer was made up of 10 neurons. The selection of the size of the second hidden layer was based on the analysis of the learning process of a set of networks of different sizes. Thanks to the incorporation of own software modules into the system, it was possible to periodically create and train networks with a given structure. Based on the results of the mean square error of network testing with different structures saved in text files, the graph shown in **Fig. 8** was created.

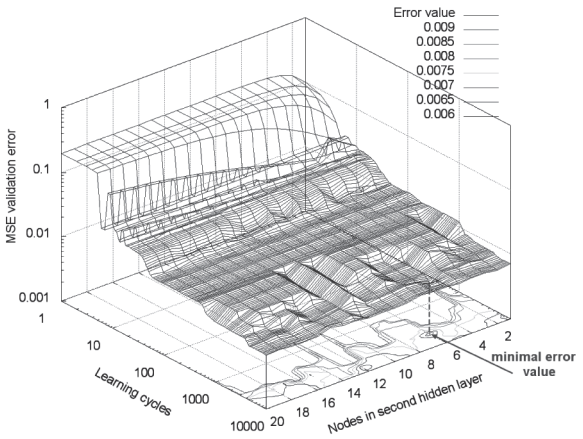

Fig. 8. Selection of the network structure
Rys. 8. Dobór struktury sieci

The network with the structure 5-10-6-1 showed the lowest value of the test error after 4,800 training cycles, therefore it was selected to create the wear model. The learning process of such a network is shown in **Fig. 9**. During learning, the values of both the learning error and the network testing error decrease, however, the learning process should be completed when the test error increases. It took place after reaching 4,800 learning cycles, which confirmed the correct selection of the parameters of the network learning process.

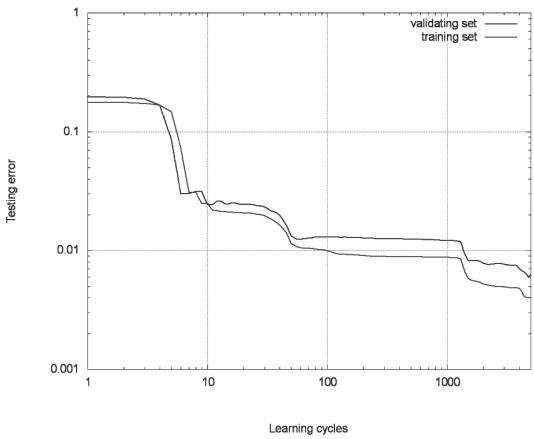

Fig. 9. Network training and testing MSE error vs. learning cycles
Rys. 9. Średniokwadratowy błąd uczenia i testowania sieci w funkcji ilości cykli

Figures 10–12 show the modelled dependencies of the specimen volume loss on the maximum Hertz pressure and the sliding distance in the contact of the three tested steels (Numbers 1, 4 and 2 from **Table 1**) with the 900A rail steel with a hardness of 34 HRC (319 HBW). These graphs show that wear increases with increasing pressure and the friction distance. The dependence of wear on pressure is close to linear. The increase in wear is due to the increase in abrasive wear. According to papers **[L. 2, 8, 24]**, adhesive wear may also occur when metallic surfaces come into contact. Increasing the pressure also intensifies it. With the increase of the sliding distance, the wear increases non-linearly – initially more intensively than with longer distances. This is mainly due to the contact geometry of the ring-block system, in which the increase of the contact area caused by wear takes place, which leads to a decrease in contact pressure **[L. 23]**.

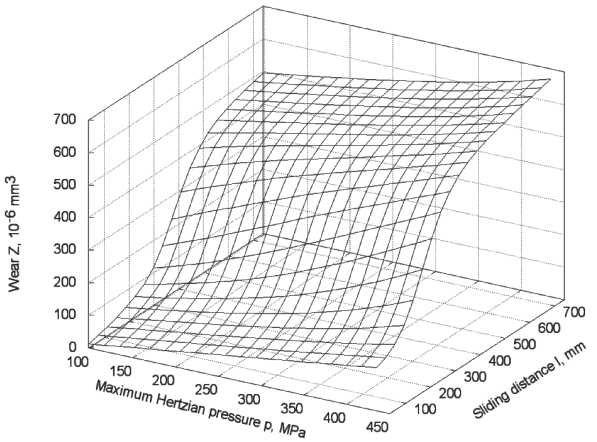

Fig. 10. Volume loss of P54 steel (hardness 203 HBW) specimen vs. maximum Hertzian pressure (p) and sliding distance (l) rubbing against 900A steel (hardness 34 HRC)

Rys. 10. Zależność zużycia objętościowego stali P54 (twardość 203 HBW) od maksymalnego nacisku Hertza (p) i drogi tarcia (l) w skojarzeniu ze stalą 900 A (twardość 34 HRC)

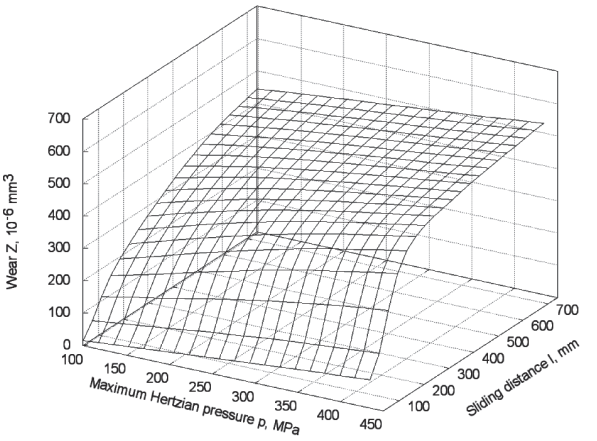

Fig. 11. Volume loss of P60 steel (hardness 280 HBW) specimen vs. maximum Hertzian pressure (p) and sliding distance (l) rubbing against 900A steel (hardness 34 HRC)

Rys. 11. Zależność zużycia objętościowego od maksymalnego nacisku Hertza i drogi tarcia dla stali P60 (twardość 280 HBW) w skojarzeniu ze stalą 900 A (twardość 34 HRC)

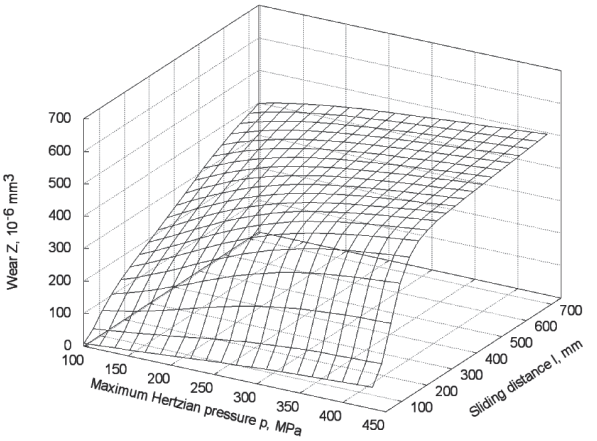

Fig. 12. Volume loss of specimen vs. maximum Hertzian pressure (p) and sliding distance (l) for P54 steel (hardness 292 HBW) rubbing against 900A steel (hardness 34 HRC)

Rys. 12. Zależność zużycia objętościowego stali P54 (twardość 292 HBW) od maksymalnego nacisku Hertza (p) i drogi tarcia (l) w skojarzeniu ze stalą 900 A (twardość 34 HRC)

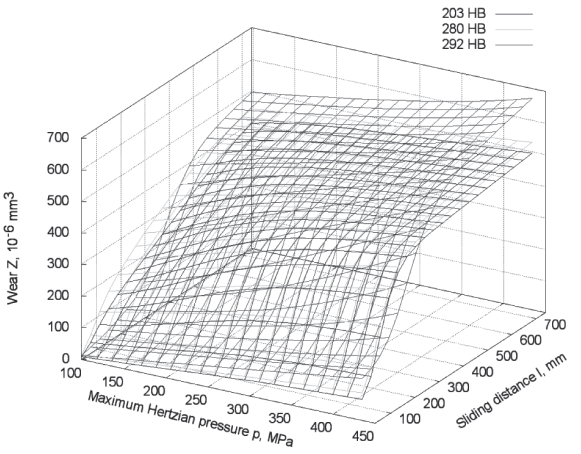

Fig. 13. Volume loss of the tested tyre steels specimens vs. maximum Hertzian pressure, sliding distance and hardness rubbing against 900A steel (hardness 34 HRC)

Rys. 13. Zależność zużycia objętościowego badanych stali obręczowych od `maksymalnego nacisku Hertza, drogi tarcia i twardości w skojarzeniu ze stalą 900 A (twardość 34 HRC)

The effect of specimen hardness on its wear while sliding on 900A steel is shown in **Fig. 13**. It presents the

obtained dependencies on a common graph. As can be seen in this figure, the greater the hardness of the tested steels, the lower their wear. This is a known regularity that is taken into account, for example, in Archard's model. Minor deviations from this rule, occurring at low values of the sliding distance, may result from the scatter of test results caused by a different course of the running-in process of the cooperating elements.

The sliding wear of 4 tested tyres steels in cooperation with a bearing steel 100Cr6 with a hardness of 61 HRC vs. maximum Hertzian pressure and sliding distance is shown in **Figs. 14–17**. As can be seen from these drawings, this wear is several times higher than in the case of sliding against rail steel of much lower hardness. It also increases with increasing pressure and friction distance. With a significant difference in the hardness of the mating materials, the dominant wear mechanism is probably the abrasive wear. The increase in pressure intensifies microcutting, which is a wear mechanism leading to a high wear rate. Hence, the relationship between wear and pressure is not linear. The high pressure during the early stage of rubbing causes

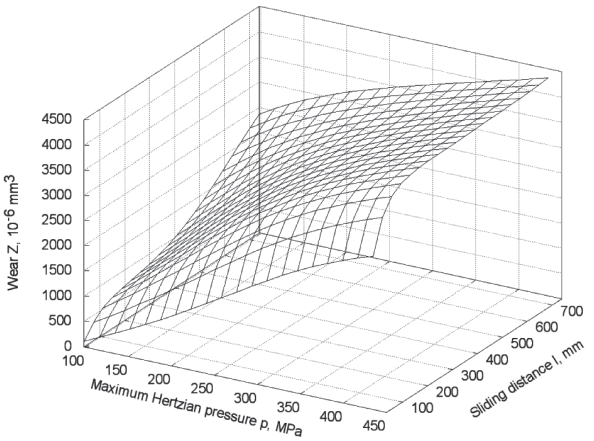

Fig. 14. Volume loss of P54 steel (hardness 203 HBW) specimen vs. maximum Hertzian pressure and sliding distance sliding against 100Cr6 steel (hardness 61 HRC)

Rys. 14. Zależność zużycia objętościowego stali P54 (twardość 203 HBW) od maksymalnego nacisku Hertza i drogi tarcia w skojarzeniu ze stalą 100Cr6 (twardość 61 HRC)

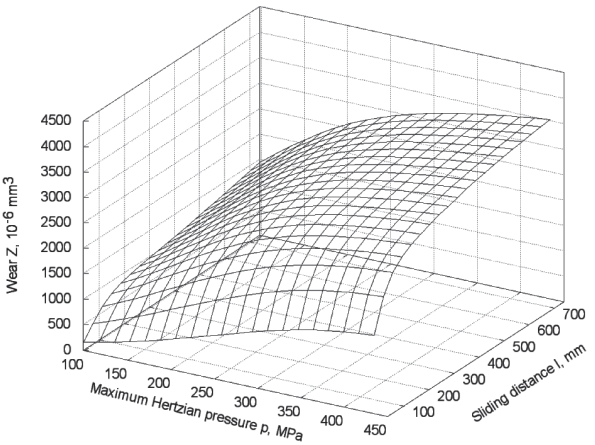

Fig. 15. Volume loss of P55A steel (hardness 247 HBW) specimen vs. maximum Hertzian pressure and sliding distance sliding against 100Cr6 steel (hardness 61 HRC)

Rys. 15. Zależność zużycia objętościowego stali P55A (twardość 247 HBW) od maksymalnego nacisku Hertza i drogi tarcia w skojarzeniu ze stalą 100Cr6 (twardość 61 HRC)

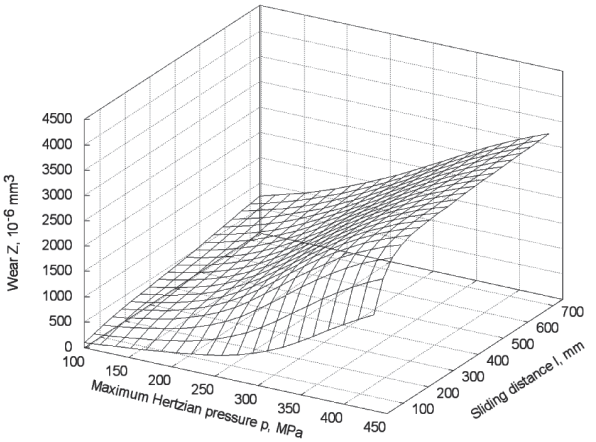

Fig. 16. Volume loss of P60 steel (hardness 280 HBW) specimen vs. maximum Hertzian pressure and sliding distance sliding against 100Cr6 steel (hardness 61 HRC)

Rys. 16. Zależność zużycia objętościowego stali P60 (twardość 280 HBW) od maksymalnego nacisku Hertza i drogi tarcia w skojarzeniu ze stalą 100Cr6 (twardość 61 HRC)

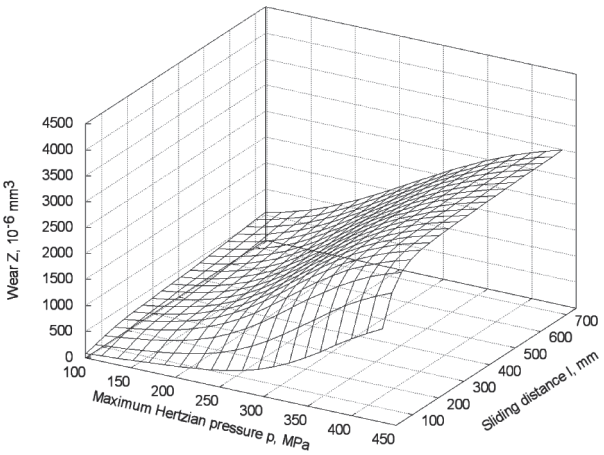

Fig. 17. Volume loss of P54 steel (hardness 292 HBW) specimen vs. maximum Hertzian pressure and sliding distance sliding against 100Cr6 steel (hardness 61 HRC)

Rys. 17. Zależność zużycia objętościowego stali P54 (twardość 292 HBW) od maksymalnego nacisku Hertza i drogi tarcia w skojarzeniu ze stalą 100Cr6 (twardość 61 HRC)

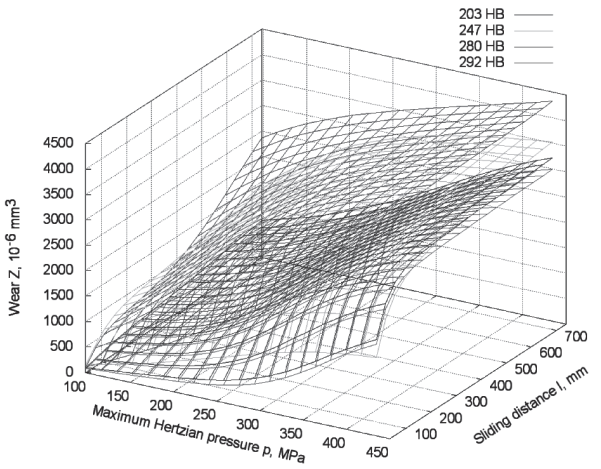

Fig. 18. Volume loss of tyre steels specimen vs. maximum Hertzian pressure, sliding distance and hardness sliding against 100Cr6 steel (hardness 61 HRC)

Rys. 18. Zależność zużycia objętościowego badanych stali obręczowych od maksymalnego nacisku Hertza, drogi tarcia i twardości w skojarzeniu ze stalą 100Cr6 (twardość 61 HRC)

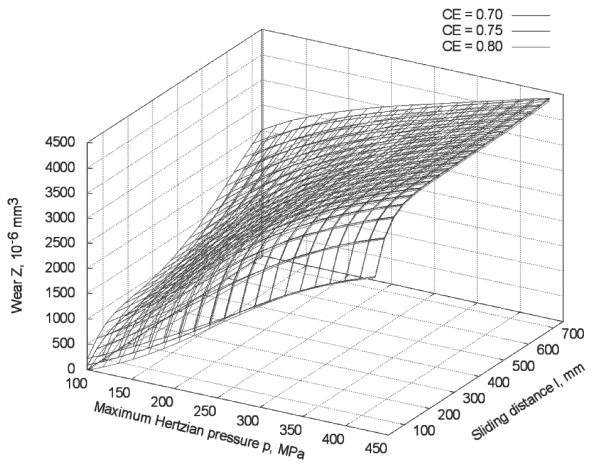

Fig. 19. Volume loss of tyre steels with hardness of 203 HBW specimen vs. maximum Hertzian pressure, sliding and carbon equivalent sliding against 100Cr6 steel (hardness 61 HRC)

Rys. 19. Zależność zużycia objętościowego stali obręczowych o twardości 203 HBW od maksymalnego nacisku Hertza, drogi tarcia i równoważnika węgla w skojarzeniu ze stalą 100Cr6 (twardość 61 HRC)

very intense wear, which makes the volume loss reach significant values even for the smallest of the tested sliding distance. The aforementioned pressure drop with increasing wear causes the wear to increase slower and slower with increasing sliding distance.

Figure 18 shows the effect of hardness on the wear of tested materials. As can be seen in this figure, their wear decreases with increasing hardness of the tested steels. Similarly, as before, the scatter of the results of wear measurements causes slight disturbances of this regularity with low values of the friction distance for some materials. **Figure 19** shows the effect of the chemical composition of steel (with the same steel hardness equal to 203 HBW) on their wear. As can be seen from the figure, this impact is small. The greater the carbon equivalent, the smaller is the wear.

CONCLUSIONS

Modelling of tyre steel wear using artificial neural networks, used in the research described in this work, allowed for the assessment of its dependence on the selected rubbing conditions and material parameters. It was found that all considered factors, i.e. the pressure, the sliding distance and the hardness of both cooperating materials, and to a lesser extent than the chemical composition of the steel expressed by the carbon equivalent influence the studied wear. During the sliding of the tested steels against the rail steel, the main wear mechanisms are abrasive wear and spalling. The first is dominant during the running-in which is at the beginning of the rubbing (with small sliding distance), while the second one is dominant for the larger distances. For spalling occurrence, it is necessary to deform the material and initiate and grow cracks (crack initiation and growth). Increasing the hardness of the material increases its resistance to both abrasive wear and spalling. Therefore, the harder the material, the less it wears. During rubbing of the tested steels against the counter-specimen of much higher hardness, an intensive type of abrasive wear, i.e. micro-cutting, dominates. Increasing the pressure causes an increase of its intensity. An increase in hardness or carbon content has the opposite effect, with the first property of the material having a greater impact on the reduction of wear, as the range of permissible carbon contents in tyre steels is smaller than in the case of hardness. In this paper, the possibility of assessing the durability of railway wheel tyres based on the results of sliding wear tests was not studied. This requires further research.

REFERENCES

1. Lewis R., Christoforou P., Wang W.J., Beagles A., Burstow M., Lewis S.R.: Investigation of the influence of rail hardness on the wear of rail and wheel materials under dry conditions (ICRI wear mapping project). Wear 430–431, 2019, pp. 383–392.
2. Prates Ferreira de Almeida L., Entringer Falqueto L., Goldenstein H., Bozzi A. C., Scandian Ch.: Study of sliding wear of the wheel flange – Rail gauge corner contact conditions: Comparative between cast and forged steel wheel materials. Wear 432–433, 2019, pp. 102894.
3. Shebani A., Iwnicki S.: Prediction of wheel and rail wear under different contact conditions using artificial neural networks. Wear 406–407, 2018, pp. 173–184.
4. Jin Y., Ishida M., Namura A.: Experimental simulation and prediction of wear of wheel flange and rail gauge corner. Wear 271, 2011, pp. 259–267.
5. Hasan S.M., Chakrabarti D., Singh S.B.: Dry rolling/sliding wear behaviour of pearlitic rail and newly developed carbide-free bainitic rail steels. Wear 408–409, 2018, pp. 151–159.
6. Chen Y., Ren R., Pan J., Pan R., Zhao X.: Microstructure evolution of rail steels under different dry sliding conditions: A comparison between pearlitic and bainitic microstructures. Wear 438–439, 2019, pp. 203011.
7. Chen Y., Ren R., Zhao X., Chen Ch., Rui Pan R.: Study on the surface microstructure evolution and wear property of bainitic rail steel under dry sliding wear. Wear 448–449, 2020, pp. 203217.
8. Viana T.G., Tressia G., Sinatora A.: Sliding Wear of Rail and Wheel Steels: Effect of Hardness Ratio, Normal Load and Lubrication. Tribology in Industry 42 No. 3, 2020, pp. 428–442.
9. Lewis R., Olofsson U.: Mapping rail wear regimes and transitions. Wear 257 (2004), pp. 721–729.
10. Hu Y., Zhou L., Ding H.H., Lewis R., Liu QY., Guo J., Wang WJ.: Microstructure evolution of railway pearlitic wheel steels under rolling-sliding contact loading. Tribology International 154, 2021, pp. 106685.
11. Robles Hernández F.C., Demas N.G., Davis D.D., Polycarpou A.A., Maal L.: Mechanical properties and wear performance of premium rail steels. Wear 263, 2007, pp. 766–772.
12. Hernández F.C.R., Demas N.G., Gonzales K., Polycarpou A.A.: Correlation between laboratory ball-on-disk and full-scale rail performance tests. Wear 270, 2011, pp. 479–491.
13. Fukagai S., Brunskill H.P., Hunter A.K., Dwyer-Joyce R.S., Lewis R.: Transitions in rolling-sliding wheel/rail contact condition during running-in. Tribology International 149, 2020, pp. 105679.
14. Lee K.M., Polycarpou A.A.: Microscale experimental and modeling wear studies of rail steels. Wear 271, 2011, pp. 1174– 1180.
15. Ramalho A. Wear modelling in rail–wheel contact. Wear 330-331, 2015, pp. 524–532.
16. Ding H.H., Fu Z.K., Wang W.J., Guo J., Liu Q.Y., Zhu M.H.: Investigation on the effect of rotational speed on rolling wear and damage behaviors of wheel/rail materials. Wear 330–331, 2015, pp. 563–570.
17. Fasihi P., Kendall O., Abrahams R., Mutton P., Lai Q., Qiu C., Yan W.: Effect of graphite and MoS2 based solid lubricants for application at wheel-rail interface on the wear mechanism and surface morphology of hypereutectoid rails. Tribology International 157, 2021, pp. 106886.
18. Adamiec P., Dziubiński J., Bąkowski H.: Ocena ilościowa procesu zużycia stali szynowej obrobionej cieplnie,. Zeszyty Naukowe Politechniki Śląskiej – Transport 56, 2004, pp. 7–15.
19. Bąkowski H., Adamiec P., Okrajni J., Posmyk A.: Ocena zużycia w styku toczno-ślizgowym. Zeszyty Naukowe Politechniki Śląskiej – Transport 57, 2005, pp 17–24.
20. Bąkowski H.: Wpływ wybranych czynników eksploatacyjnych na zużycie elementów skojarzenia toczno--ślizgowego w obecności płynu. Zeszyty Naukowe Politechniki Śląskiej, Transport 64, 2008, pp. 71–76.
21. Witaszek M., Bąkowski H.: The influence of dry, rolling-sliding friction conditions on the wear of a rail steel mated with hardened tyre steel. Tribologia 213, 2007, pp. 389–400.
22. Bąkowski H., Posmyk A.: Wpływ wybranych parametrów eksploatacji na właściwości tribologiczne skojarzenia toczno-ślizgowego. Tribologia 218, 2008, pp. 35–41.
23. Sundh J., Olofsson U.: Relating contact temperature and wear transitions in a wheel–rail contact. Wear 271, 2011, pp. 78–85.
24. Viáfara C.C, Castro M.I., Vélez J.M., Toro A.: Unlubricated sliding wear of pearlitic and bainitic steels. Wear 259, 2005, pp. 405–411.
25. Bąkowski H., Służałek G.: Wpływ obciążenia i prędkości obrotowej na zużycie stali bainitycznej w skojarzeniu ślizgowym na stanowisku Amslera. Tribologia 225, 2009, pp. 11–18.
26. Ki Myung Lee, Polycorpou A.A.: Wear of conventional pearlitic and improved bainitic steels. Wear 259, 2005, pp. 391–399.
27. Boyacioglu P., Bevan A.: Prediction of rail damage using a combination of Shakedown Map and wheel-rail contact energy. Wear 460-461, 2020, pp. 203457.
28. Clayton P.: The relations between wear behavior and basic material properties for pearlitic steels. Wear 60, 1980, pp. 75–93.